Benefits of the Adaptive Algorithm for Retracking Altimeter Nadir Echoes: Results From Simulations and CFOSAT/SWIM Observations

Cédric Tourain, Fanny Piras, Annabelle Ollivier, Danièle Hauser, *Member, IEEE*, J. C. Poisson, F. Boy, P. Thibaut, L. Hermozo, and C. Tison

***Abstract*— The accuracy of sea surface parameters retrieved from altimeter missions is predominantly governed by the choice of the so-called "retracking" algorithm, i.e., the model and inversion method implemented to obtain the surface parameters from the backscattered waveform. For continuity reasons, the choice of space agencies is usually to apply the same retracker from one satellite mission to the other to ensure long-time homogeneous series. In this article, taking the opportunity of a new configuration of the nadir pointing measurements onboard the recently launched China France Oceanography Satellite (CFOSAT) with the Surface Waves Investigation and Monitoring (SWIM) instrument (Hauser *et al.,* 2020), the retracking method was upgraded, by implementing a novel algorithm, called "Adaptive" retracker. It combines the improvements brought by Poisson *et al.,* (2018) for the estimation of surface parameters from peaked waveforms over sea ice, improvements in the way the instrumental characteristics are considered in the model (mispointing, point target response) and a more accurate consideration of speckle statistics. In this article, we first show from simulations carried out in the instrumental configuration of SWIM that the Adaptive algorithm has better accuracy and performance than the classical MLE4 algorithm. Then, the geophysical parameters obtained with real data from SWIM are analyzed with comparisons to reference data sets (model and products from altimeters). We show that this new algorithm has several benefits with respect to the classical MLE4 method: no need of lookup tables to correct biases, significant noise reduction on all geophysical variables especially the significant wave height, and performance of inversion over a large set of echo shapes, resulting from standard oceanic scenes as well as highly specular conditions such as over bloom or sea ice.**

***Index Terms*— Altimetry, China France Oceanography Satellite (CFOSAT), nadir, ocean, radar, retracking algorithm, Surface Waves Investigation and Monitoring (SWIM), validation.**

Manuscript received November 18, 2020; revised January 27, 2021; accepted February 15, 2021. *(Corresponding author: Cédric Tourain.)*

Cédric Tourain, F. Boy, and C. Tison are with the Radar Processing and Products Department, Centre National d'Etudes Spatiales, 31401 Toulouse, France (e-mail: cedric.tourain@cnes.fr).

Fanny Piras, Annabelle Ollivier, J. C. Poisson, and P. Thibaut are with Collecte Localisation Satellites SA, 31400 Ramonville Saint-Agne, France.

Danièle Hauser is with LATMOS, Centre National de la Recherche Scientifique, 75794 Paris, France.

L. Hermozo is with DCT/SI/IP, Centre National d'Etudes Spatiales, 31401 Toulouse, France.

Color versions of one or more figures in this article are available at https://doi.org/10.1109/TGRS.2021.3064236.

Digital Object Identifier 10.1109/TGRS.2021.3064236

I. Introduction

IN SATELLITE altimetry, the return echo results from a series of pulses reflecting the Earth's surface. Geophysical variables are obtained from the on-ground processing by inversion of the backscattered echo, using a method called ≪ retracking ≫. For observations over the sea surface, this method fits an analytical model described in [1] as the convolution of a point target response (PTR), a flat sea surface response (FSSR), and the probability density function (pdf) of the scattering elements of the elevations. Historically, the first retracking method used for oceanic surfaces was the so-called MLE3 [2] providing three parameters: the epoch, defined as the position of the signal in the analysis window with respect to the tracking reference point (which is then converted in sea surface height SSH), the normalized radar cross section σ^0, and the significant wave height (SWH). After the launch of Jason-1 in 2001 and to better account for attitude effects, the MLE4 was introduced [3], providing the same three parameters as the MLE3, plus the slope of the trailing edge of the waveform. However, these retracking algorithms show several known limitations. The major one is the need for lookup tables (LUTs) [4] to compensate for the error made by modeling the PTR by a Gaussian function. Furthermore, the likelihood function used in the estimator is equivalent to an unweighted least square estimator (LSE) [2], [4]. This means that the optimization does not properly account for the speckle noise statistics impacting the waveform and introduces significant noise on the retrieved parameters.

The state of the art of retracking methods also covers improvements dedicated to nonwater surfaces. ICE-1 is based on the offset center of gravity (OCOG) method [5]; it proves robust for nonstandard waveforms such as those frequently encountered over continental waters [6]. Its outputs are limited to range and σ^0. ICE-2 [7] is based on the fitting of a simplified Brown model [1] around the leading edge for classical ocean geophysical parameter, and ice and land-oriented parameters estimation based on the trailing of the waveform. It provides information over land and ice surfaces. However, over ocean, performances are lower than ocean-oriented retrackers (such as MLE3 and MLE4). ALES [8] is designed to be applied both over open and coastal ocean, as it adapts the width of the subwaveform according to the SWH.

A new algorithm, named "Adaptive," was developed in [9] for ENVISAT data processing to improve the continuity of performances of sea-level inversion between open ocean and arctic leads. One of its key advantages is the introduction of the mean-square surface slope of the dominating reflective surface (mss) as a parameter influencing the trailing edge of the echo. This better constrains the retrieval of the normalized backscatter (which is related to mss in specular backscattering conditions) and provides better fits on echoes from highly reflective surfaces such as sea ice. Finally, the estimation procedure proposed in [9] allows to better account for speckle noise characteristics. This is important for all altimeter missions but even more important for Surface Waves Investigation and Monitoring (SWIM) because of its relatively lower sampling rate of downloaded waveform (4.5 Hz instead of 20 Hz in standard altimeter missions) and hence lower spatial resolution and noisier compressed 1-Hz data.

In this article, we propose a modified version of the Adaptive retracking method mentioned in [9], by extending its model to consider the real PTR of the altimeter measured in-flight. We also propose another improvement on the approach mentioned in [9] by using the mispointing as an input variable, motivated by the specific configuration of the SWIM instrument onboard the recently launched China France Oceanography Satellite (CFOSAT) mission [10], [11], which provides a systematic estimation of mispointing angles estimated from the off-nadir observations that can be directly used for the nadir pointing observations Adaptive retracking.

This article aims at demonstrating the interest and showing the performances of this algorithm. It is illustrated with CFOSAT/SWIM nadir data, but conclusions are more general.

In the following, we will present a performance analysis of this novel Adaptive retracking algorithm based on both simulated and real data sets. As the SSH is not a variable to be provided to users in SWIM products, this article focuses on SWH and σ^0.

This article is organized as follows. In Section II, the main characteristics of SWIM and its raw data are summarized. In Section III, we recall the theoretical background of the current retracking algorithms (used in ground segments of space agencies) and present the modifications brought by the Adaptive retracking. Then, in Section IV, simulation results obtained for an observation configuration similar to SWIM are discussed to illustrate the improvements brought by the Adaptive algorithm, in comparison to the MLE4 algorithm. In Section V, the performances of the Adaptive algorithm are assessed on SWIM real data by comparing results from the Adaptive and the MLE4 methods. In Section VI, SWIM geophysical products obtained with the Adaptive algorithm are compared to model outputs and altimeter products at crossover points to assess their performance with respect to independent data sets. We finally conclude and give perspectives in Section VII.

II. SWIM Nadir Mode Configuration

The CFOSAT program [10] is carried out through cooperation between the French and Chinese Space Agencies (CNES and CNSA, respectively). It aims at characterizing the ocean surfaces to better model and predict the ocean states and improve the knowledge in ocean/atmosphere exchanges. Data over continental surface are also available for studies on continent.

The CFOSAT satellite was launched on October 29, 2018 with onboard two scientific Ku-band radars: SWIM, a nadir and near-nadir wave scatterometer [11], and SCAT, a wind scatterometer [12]. CFOSAT has a sun synchronous orbit repetitive with a 13-day cycle, its altitude and inclination are, respectively, 520 km and 97.4°. Although CFOSAT is not a standard altimeter mission, SWIM instrument includes a nadir pointing designed to measure SWH and σ^0 as classically carried out from other altimeter missions. In contrast, neither the epoch nor SSH was specified as a variable to be provided to users. SWIM has also five beams pointing near nadir to estimate directional spectra of ocean waves [11], [13]. The six beams illuminate the surface sequentially at 0°, 2°, 4°, 6°, 8°, and 10° incidence with respect to nadir, with a scanning geometry (see [11], [13]). Due to this specificity, the nadir waveform sampling is slightly different from standard altimeter missions; although the number of raw samples considered in the onboard integrated echo is larger than that of standard altimeter missions (264 instead of 90 for Jason missions), the mean waveform after onboard processing is provided at a 4.5-Hz rate, instead of the usual 20 Hz in standard altimetry. This is because time is reserved for the acquisition of the signal on the nonnadir beams. This means that the native data cannot be analyzed at high (∼20 Hz) frequency and that the noise on the postprocessed mean values provided at 1 Hz are larger than for other altimeter missions (for the same instrument characteristics). Therefore, specific effort must be done to avoid additional noise on the retrieved parameters due to the inversion.

Another feature of SWIM onboard CFOSAT is that the mispointing angle is provided, as ancillary information, by the off-nadir beam at the same frequency as the waveform (4.5 Hz). The method to estimate the mispointing is explained in [13]. This information is particularly important for SWIM as it was shown [13] that the mispointing varies slightly with the look angle during the rotation of the feed horn plateau.

III. Theoretical Background on Nadir Retracking and Description of the Adaptive Method

The general principle of usual retracking algorithms [1] is to fit a waveform model to the real signal received by the instrument. The inversion (hereafter called estimation procedure) is carried out by using minimization of a likelihood function, which characterizes the distance between model and observations.

In this section, we recall the historical background for both the MLE4 and the Adaptive method and describe the choices for the inversion procedure.

A. Theoretical Background and MLE4 Echo Model

Here, we first describe the theoretical background for the model used in the commonly used retracker for oceanic

surfaces (MLE4), and then, the specificities of the Adaptive model are detailed in Section III-B.

The signal $S(t)$ received by the instrument is given by the following double convolution [1], [15]:

$$S(t) = \mathrm{FSSR}(t) * \mathrm{PDF}(t) * \mathrm{PTR}(t) \tag{1}$$

where FSSR is the flat sea surface response, PDF is the surface elevation pdf of scattering elements, PTR is the radar system PTR, and $*$ is a convolution product.

1) PDF: PDF(t) Function: The surface elevation pdf of scattering elements is given in [16, eq. (I.28)], considering a fourth-order development

$$\mathrm{PDF}(\eta) = \frac{1}{\sqrt{2\pi\sigma_s^2}}\exp\left(-\frac{\eta^2}{2}\right) \times\left[1+\frac{\lambda s}{6}\left(\eta^2-3\eta\right)+\frac{\kappa s}{24}\left(\eta^4-6\eta+3\right)\right] \tag{2}$$

where η is the height normalized by the standard deviation of wave heights σ_s [16], [17]. It is also characterized by the skewness λ_s (third-order moment) and the kurtosis κ_s (fourth-order moment). Brown [1] approximated this expression by a Gaussian model with $\lambda_s = 0$ and $\kappa_s = 0$. Hayne [15] used a nonnull skewness coefficient λ_s.

2) PTR: PTR(t) Function: The radar PTR is generally expressed as a square sinc function that results from the deconvolution of the emitted chirp (linear modulation of the frequency with respect to the time) [3]

$$\mathrm{PTR}(t) = \left|\frac{\sin\left(\pi\frac{t}{Ts}\right)}{\pi\frac{t}{Ts}}\right|^2 \tag{3}$$

where $Ts = 1/B$ is the sampling period and B is the radar system reception bandwidth.

Brown [1] approximated this expression by a Gaussian model, which according to [3] and [16], [17] leads to

$$\mathrm{PTR}(t) = \frac{1}{\sqrt{2\pi}\sigma_p}\exp\left(\frac{-t^2}{2\sigma_p^2}\right) \tag{4}$$

with $\sigma_p = 0.513Ts$ related to the PTR width at -3 dB [18].

3) FSSR Model: FSSR(t) Function: The final formulation of the model commonly used in conventional altimetry is derived from the Brown model [1]. In this formulation, the flat sea surface impulse response in (1) is given by

$$\mathrm{FSSR}(t) = \mathrm{AP}\exp\left[-\frac{ct}{h}\left(\frac{4}{\gamma}\cos 2\xi+\alpha\right)\right] I_0\left(\beta t^{1/2}\right) \tag{5}$$

where

$$A = \exp\left(\frac{-4\sin^2\xi}{\gamma}\right)$$

$\gamma = (2/\ln(2)).\sin^2(\theta_0/2)$ with θ_0: 3-dB antenna beamwidth, P is the amplitude of the signal, h is the satellite altitude, ξ is the absolute off-nadir pointing angle, α is a function of the radar observed surface characteristics, mainly the mean-square slope, and I_0 is the Bessel function

$$\beta = \frac{4}{\gamma}\left(\frac{c}{h}\right)^{1/2}\sin 2\xi.$$

Hayne [15] ignored the α parameter, assuming that sea surface roughness cannot be null. The expression is then simplified from (5) to (6)

$$\mathrm{FSSR}(t) = \mathrm{AP}\exp\left[-\frac{ct}{h}\left(\frac{4}{\gamma}\cos 2\xi\right)\right] I_0\left(\beta t^{1/2}\right). \tag{6}$$

The final formulation of the return power, considering the skewness coefficient and a Gaussian approximation of the PTR, is an analytical model described in [15] and [16], [17] and is the one used in the ground segments of space agencies for the MLE4 algorithm.

B. Adaptive Echo Model

The formulation proposed in [15] shows the limitations in the case of sea ice and leads. Based on the FSSR model developed by Amarouche *et al.* [19] and Amarouche and Vernier [20], a modified formulation of the FSSR was proposed in [9]

$$\mathrm{FSSR}(t) = \mathrm{AP}\exp\left[-\frac{ct}{h}\left(\frac{4}{\Gamma}\right)\right] I_0\left(\beta t^{1/2}\right) \tag{7}$$

where

$$\Gamma = \frac{4\gamma\ \mathrm{mss}}{4\mathrm{mss}+\gamma} \tag{7a}$$

and mss is the mean square slope.

The main evolution in this model with respect to the most classical expression of (6) is that surface characteristics effects are considered through the mss parameter in the exponential parameter (and not only through the amplitude of the signal), allowing far greater flexibility to adapt to specular echoes (see Section IV). Indeed, contrary to the Haynes model (6) that constrains its trailing edge with the off-nadir angle only, this approach allows the trailing edge of the echo to be also constrained by the surface roughness.

To do so, the Amarouche model uses the following σ^0 modeling:

$$\sigma^0(\theta) = \sigma^0(0)\exp\left(-\frac{\sin^2(\theta)}{\mathrm{mss}}\right) \tag{8}$$

where σ^0 is the normalized cross section, proportional to the amplitude P of the signal, θ is the incidence angle from nadir, and mss is the mean-square surface slope of the dominating reflective surface in the altimeter footprint [9]. However, this formulation, as used in [9], does not consider the off-nadir angle, contrary to the original Brown model [1].

Therefore, we propose to use the full expression of the Adaptive model as described in [19], allowing to specify the mispointing as an input. Equation (7) stays as it is but with the Γ parameter replaced by

$$\Gamma = \frac{4\gamma\ \mathrm{mss}}{4\,\mathrm{mss}\cos 2\xi+\gamma}. \tag{9}$$

Equation (9) is equivalent to (7a) when the mispointing angle is neglected.

As explained in [9], it is assumed that even the most reflective surfaces such as sea-ice leads have a nonnull surface roughness, meaning that the parameter mss in (9) can never be equal to zero.

Finally, the formulation of the analytical model used in the Adaptive model is reduced to the following sea surface response (SSR):

$$\mathrm{SSR}(t) = \frac{A\sigma_0}{2}\left[1 + \mathrm{erf}\left(\frac{t - \tau - \frac{4c}{\Gamma h}\sigma_s^2}{\sqrt{2}\sigma_s}\right)\right] \times \exp\left[-\frac{4c}{\Gamma h}\left(t - \tau - \frac{2c}{\Gamma h}\sigma_s^2\right)\right] + N_t \quad (10)$$

where τ is the epoch and N_t is the additive thermal noise.

Compared to [9, eq. (5)], the composite variable σ_c of [9] $\left(\sigma_c = \left(\sigma_s^2 + \sigma_p^2\right)^{1/2}\right)$ is replaced by σ_s, by imposing a null value of the PTR-related variance σ_p^2. The analytical model expression is reduced to the only convolution of the FSSR with the PDF, called SSR. The model expression (1) can then be expressed as the convolution of the PTR with SSR: $S(t) = \mathrm{SSR}(t) * \mathrm{PTR}(t)$. In the context of the Adaptive retracking, this convolution is performed numerically.

The final formulation of the model used in the Adaptive retracking, hereafter called the "Adaptive model," is therefore a semianalytical model based on the analytical expression (10) and a numerical PTR.

C. Likelihood Function and Minimization Procedure

The most commonly used minimization procedures are based on a likelihood estimator [such as maximum likelihood estimator (MLE)] in order to consider noise associated with the data in the inversion process.

Indeed, radar data are corrupted by multiplicative speckle noise. To reduce the impact of this noise affecting each individual echo, a sequence of consecutive pulses is averaged onboard. Assuming pulse-to-pulse statistical independence, the resulting speckle noise follows a Gamma distribution depending on the number N of averaged individual pulses. A likelihood function can be derived from these statistics [21] and is expressed as

$$C = \mathrm{cst} + N\sum_{k=0}^{K-1}\frac{y_k}{S_k} - (N-1)\sum_{k=0}^{K-1}\ln(y_k) + N\sum_{k=0}^{K-1}\ln(S_k) \quad (11)$$

where y_k is the measured waveform, S_k is the model, k is the waveform sample number within K samples, and cst is a constant.

In common conventional altimetry processing such as the MLE4, a simplification of (11) is often applied following expression (12), which is a more classical LSE:

$$C = \sum_{k=0}^{K-1}(y_k - S_k)^2. \quad (12)$$

This is not optimal as it does not account for noise properties of the measured variable and this can have an impact on the final noise on the retrieved parameters.

D. Adaptive Algorithm for CFOSAT/SWIM

The first specificity of the algorithm selected for SWIM is to choose the Adaptive echo model from (10) with the parameter Γ given by (9), considering a Gaussian model for the surface elevation pdf [null skewness λ_s and kurtosis $\mathfrak{s}_s$ in (2)]. When applied on the SWIM real data, the mispointing angle ε is fixed from off-nadir angle estimations provided independently of the off-nadir beam observations of SWIM (see [13]). Parameters estimated are thus: the epoch τ, the standard deviation of wave heights σ_s, the amplitude of the signal P, and the mean-square slope mss.

The second specificity of the algorithm proposed here is that we choose to use the real in-flight PTR of the instrumental, by convolving its discretized values numerically to the analytical model given by (10).

We will see further below that this choice is significant as it enables us to estimate the geophysical parameters without any bias correction to compensate for the Gaussian approximation of the PTR. Furthermore, it can consider the natural aging of the instrument and its potential effects (sides lobe dissymmetry, evolution of the position of the maximum of the PTR, and so on). Indeed, for SWIM as for most altimeters, the PTR is measured regularly through an internal calibration sequence mode [13]. Therefore, the PTR used as an input of the Adaptive model is updated along with the calibration sequences, to follow the instrument's aging as close as possible.

The third specificity is to minimize the model by using the likelihood estimator (MLE) from (11), i.e., considering the noise properties of the radar echo. This is different from most of the MLE4 algorithms implemented for the current altimeter missions, which use the simpler LSE given by (12).

A numerical scheme is required to invert the statistical estimator function. Two main algorithms are used in conventional altimetry. The first one is the Newton–Raphson algorithm. It minimizes the cost function by a gradient descent approach. The second algorithm is a geometrical method called the Nelder–Mead algorithm [22]. It is a direct search method (based on function comparison) and is often applied to nonlinear optimization problems for which derivatives may not be known.

The Newton–Raphson algorithm has the advantage of converging in a reduced number of iterations due to the gradient descent method. To do so, the cost function and its derivatives must be estimated. The Nelder–Mead algorithm needs more iterations, and however, only the cost function must be estimated, which simplifies the implementation and reduces the number of operations at each iteration.

Therefore, for SWIM nadir processing, the Nelder–Mead method has been selected as the optimization algorithm.

In the SWIM products, the outputs of this inversion are the SWH estimated from the σ_s parameter of (10) and the normalized radar backscatter σ^0, constrained by both the received power P and the Γ parameter of (6).

The improvements brought by each of these evolutions with respect to the classical MLE4 algorithm are detailed in the following.

IV. Theoretical Benefits of the Adaptive Algorithm Based on Simulations

In this section, a simulated data set is used to assess the proposed method based on (10) and (11) and to compare its performance to the more classical retracking algorithms. We consider four configurations, as detailed in Table I.

TABLE I

LIST AND SPECIFICITIES OF THE DIFFERENT RETRACKING SOLUTIONS CONSIDERED IN THE TRADEOFF

Name	Model	PTR	Likelihood criterion
MLE4	Brown	Gaussian Model	LSE
R1	Brown	Real	LSE
R2	Brown	Real	MLE
Adaptive	Adaptive	Real	MLE

TABLE II

SIMULATION PARAMETERS

Altitude (Km)	550	Amplitude (p.u)	160
Bandwidth (Hz)	320	Thermal Noise (p.u)	1.0
Sampling Freq. (Hz)	400	Skewness	-0.1
Ant. Beam (°)	1.51	Off-nadir angle (°)	0
Nb of samples	256	First useful gate	64
Ref. Abscissa	108	Last useful gate	192

A. Simulated Data Set and Method

The data set was generated by modeling waveforms based on the analytical Hayne model according to (6) convolved with a real PTR. This latter was taken from a measured PTR of SWIM dated August 27, 2019. The simulation parameters are based on the CFOSAT geometry and SWIM instrumental characteristics. They are given in Table II. Note that no mispointing is considered in these simulations. Here, we generate directly 4.5-Hz averaged waveforms, so the speckle noise is applied to model waveforms through a Gamma law $(1/N, N)$ with $N = 264$, corresponding to the real number of SWIM samples accumulated at this 4.5-Hz frequency. Simulations are generated for different SWH values (Fig. 1), from 1 to 8 m, with a step of 1 m. Roughness is considered as homogeneous in the footprint. For each step, a random draw of 10 000 gamma laws is generated and then multiplied to the modeled waveform. The thermal noise is an additive noise, and it is thus applied posterior to the speckle noise multiplication step.

The resulting data sets are then processed by the four retracking algorithms presented in Table I.

The first one corresponds to the MLE4, which is the current operational conventional altimetry retracking algorithm. Then, components are modified one after the other to observe their impact on the estimation performances.

To assess the performances of all three configurations, the following diagnoses are performed:

1) waveform residuals (the average difference between the model and the signal) for each SWH step, to assess the quality of model fitting;
2) the average bias per SWH step, i.e., the mean difference between the simulation input parameter and the result, over the 10 000 draws;
3) the estimation noise per SWH step, i.e., the mean standard deviation over the 10 000 draws.

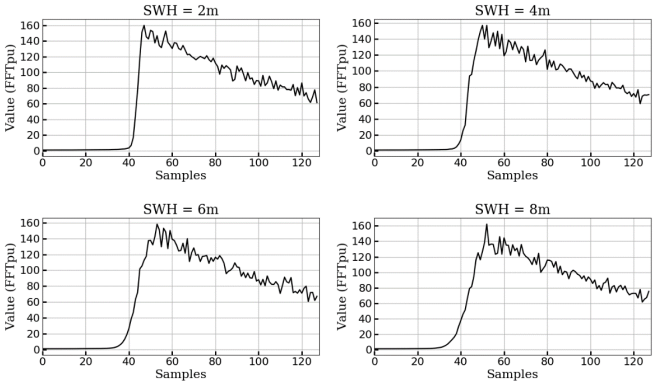

Fig. 1. Example of waveforms simulated for four SWH steps (2, 4, 6, and 8 m), after application of speckle noise and thermal noise. The Y-axis represents the amplitude in fast Fourier transform (FFT) power units.

B. Impact of the PTR: R1 Versus MLE4

As already described, the conventional operational retracking algorithm considers a modeled PTR, which implies the use of LUTs [14] to compensate for SWH and σ^0 biases. As shown in Fig. 2, consider the real PTR through a convolution (method R1, orange curves) instead of a Gaussian model (method MLE4, black curves) improves remarkably the fit of the modeled waveform with the signal.

The differences between fitted echoes and the reference waveforms are significantly smaller for the R1 case (orange curve) than for the MLE4 case (black curve)

This especially visible for the leading edge (samples from 30 to 50). Note also that according to Fig. 2, the improvement increases when SWH decreases. Retrieved mean values given in Fig. 3(a) show that with R1 (orange curve), the bias on the retrieved SWH is very low (less than 1cm), in opposite to MLE4 (blue curve). For MLE4, LUTs are computed (see Section V-A) and used to compensate for the bias observed. This interestingly shows that when using the real PTR in the convolution product, no more LUTs are needed for correcting this parameter after inversion. As for the mean value of σ^0 [see Fig. 3(b)], we observe no significant difference between the MLE4 and the R1 solution: a bias of 0.25 dB is found for both configurations. This was expected because the Gaussian approximation of the PTR has a low impact on this parameter.

C. Impact of the Likelihood Function: R1 Versus R2

As shown in Fig. 3, the implementation of the likelihood function (10) (R2 : orange curve) induces a 60% noise reduction on SWH and 11% on σ^0, with respect to an LSE (R1 : red curve). The solution with R2 also significantly reduces the bias on σ^0, providing a null bias (compared to 0.25 dB for R1). Indeed, by using the MLE likelihood criterion, the speckle law statistics is considered, allowing not only to reduce the estimation noise but also to better fit the trailing edge of the waveform, reducing the remaining small σ^0 biases to almost zero. The same effect is expected on the SWH parameter, even though it is not significant enough to be visible on these simulations. Hence, these results show that to be fully free from LUTs, the introduction of the real PTR is the most

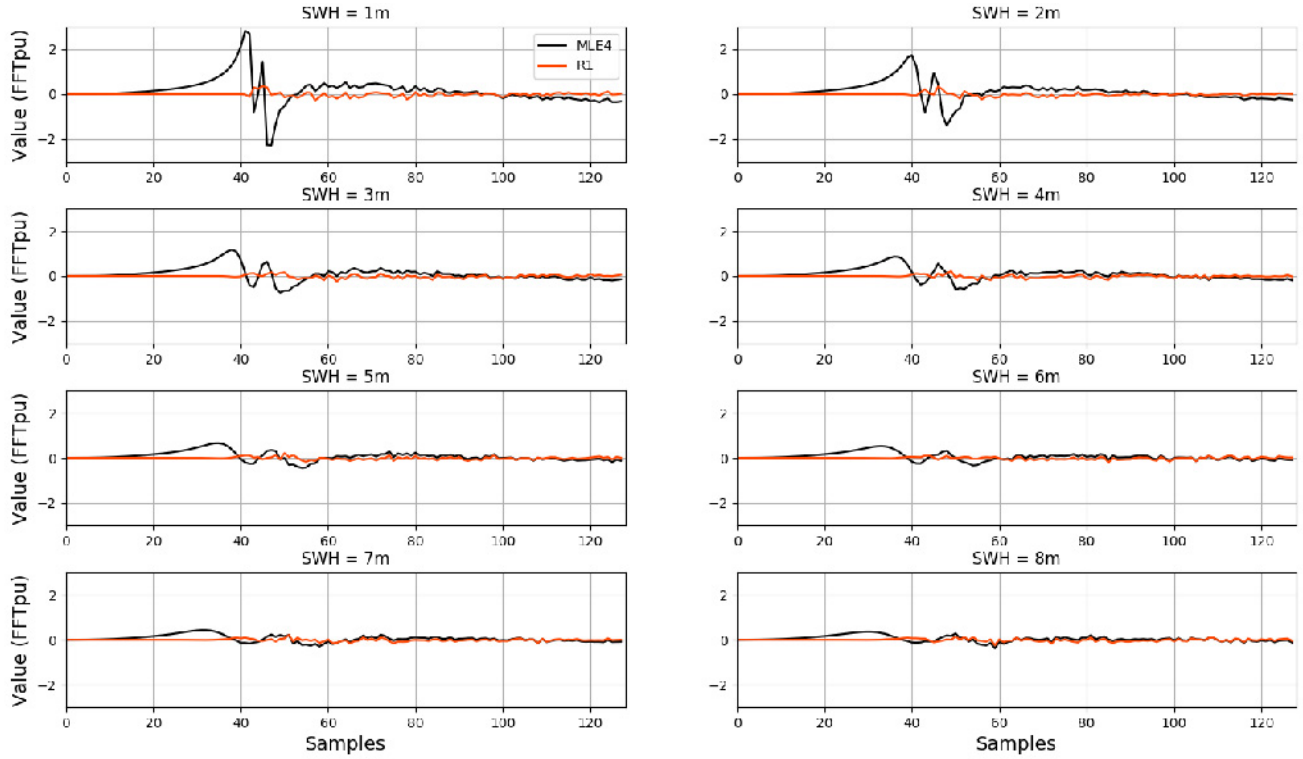

Fig. 2. Differences between fitted echoes and the reference waveforms over al1 samples for a retracking processing with MLE4 algorithm with modeled PTR convolution (black curve) and R1 retracking with real PTR convolution (red curve). The Y-axis represents the amplitude in FFT power units.

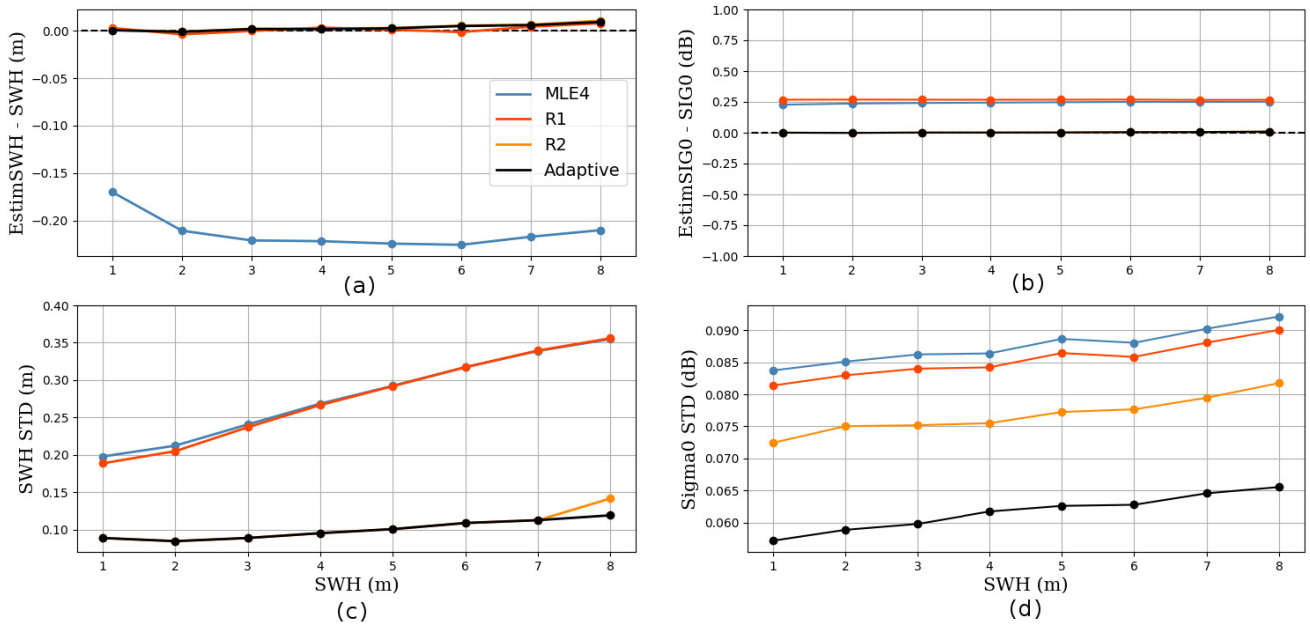

Fig. 3. (a) SWH biases, (b) σ^0 biases, (c) SWH standard deviation, (d) σ^0 standard deviation. Statistics retrieved from MLE4 (blue), R1 (red), R2 (orange), and Adaptive (black) algorithms. Note that in (c), the orange curve for R2 is hidden behind the black one.

appropriate to get rid of SWH bias, while the MLE likelihood criterion is more appropriate to get unbiased σ^0.

D. Adaptive Model Versus Brown Model: Adaptive Versus R2

Fig. 3 shows that the Adaptive (black curves) and R2 solution (yellow curves) show equivalent performances in terms of bias for both SWH and σ^0. This is expected because the main difference between the Adaptive and R2 is the introduction of the mss in the σ^0 formulation. In the case of classical oceanic echoes such as the simulated data set used in this section, the introduction of the mss has negligible impact on the biases.

The main difference is for the σ^0 rms error where a noise reduction of 20% is observed compared to R2. As explained

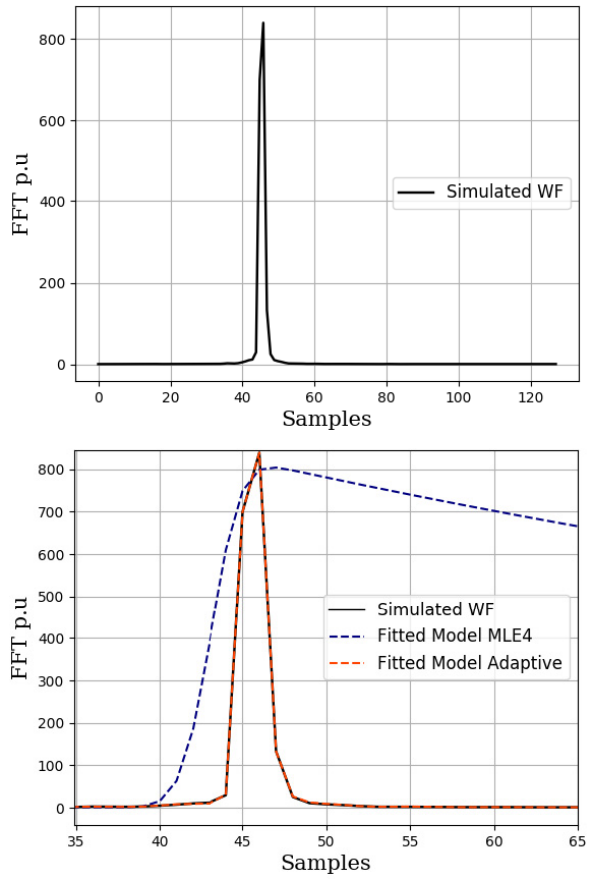

Fig. 4. (Top) Simulated peaky echo and the corresponding models for Adaptive (red) and MLE4 (blue), zoomed on (Bottom) useful part of the signal. The Y-axis represents the amplitude in FFT power units.

just before, this is due to the fact that in the Adaptive model, the σ^0 formulation considers the mss parameter (8); therefore, it is better constrained by the echo shape. In fact, the interest of the Adaptive model with respect to the Brown model is the most significant on peaky echoes processing. This is shown in Fig. 4, which shows a simulated peaky echo and the corresponding models for both MLE4 and Adaptive retracking. The MLE4, aimed at processing ocean echoes, tries unsuccessfully to fit the Brown model, whereas the Adaptive model perfectly fits the waveform, proving its ability to retrack echoes that are not typical ocean diffuse echoes.

V. Adaptive Versus MLE4: Results Obtained on Real CFOSAT Data

The different results presented above have led us to the selection of the so-called Adaptive retracking algorithm for the SWIM nadir data processing in the NRT CFOSAT ground segment. Note that Adaptive retracking refers below to the configuration described in Section III-D combined with the Nelder–Mead algorithm for the minimization process.

In this section, we compare the results obtained from the same SWIM data set using the Adaptive algorithm on one side and the MLE4 algorithm on the other side.

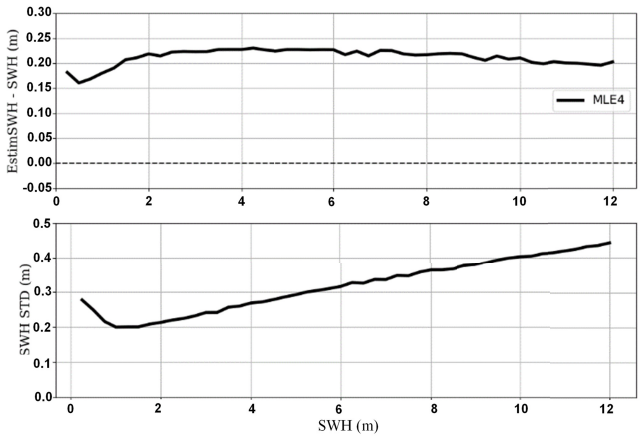

Fig. 5. MLE4 LUTs for SWH.

A. Description of the Data Used

We use here two different data sets, both obtained on 13 days of CFOSAT data (one orbital cycle): the first data set contains Adaptive retracking outputs, obtained directly from the ground-segment products. The second data set contains MLE4 retracking outputs, obtained by applying off-line the MLE4 processing on the 5-Hz nadir SWIM echoes, for the purpose of this demonstration. The cycles chosen for this analysis are cycles 5 and 16, covering, respectively, the periods from December 23, 2018 to January 5, 2019 and from May 15, 2019 to May 28, 2019.

To consider comparable data sets, SWH LUTs have been computed to compensate for the error made using a Gaussian approximation of the PTR in the MLE4 retracker. These LUTs have been computed using the simulations described in Section III-A, for SWH values from 0.25 to 12 m with a step of 0.25 m. This correction on SWH varies between 15 and 20 cm (see Fig. 5) and has been applied to the SWH MLE4 data set for the analysis presented in this section. Note that no LUTs have been computed here for the σ^0 parameter, as they are usually considered negligible and not used in the operational MLE4 products.

Results also include comparisons to models, interpolated at SWIM resolution.

B. Fit of the Waveform

To assess the quality of a retracker's waveform fit, the mean-squared error (mse), also called mean quadratic error (MQE) is computed. The comparison of MQE obtained between MLE4 and Adaptive, illustrated in Fig. 6, shows the superior Adaptive performances; on average, the Adaptive MQE is 30% lower than the MLE4 MQE with a similar standard deviation [see Fig. 6(a)]. The map of the differences [see Fig. 6(b)] displays only positive values, meaning that the Adaptive fit is an improvement compared to the MLE4, over all regions of the planet. This improvement is heterogeneous and different patterns appear, correlated with the roughness of the surface, which is a consequence of two main differences in the algorithm. First, by considering the real PTR of the instrument, the fit on the leading edge is largely improved with the Adaptive model compared to MLE4 (Fig. 2) in

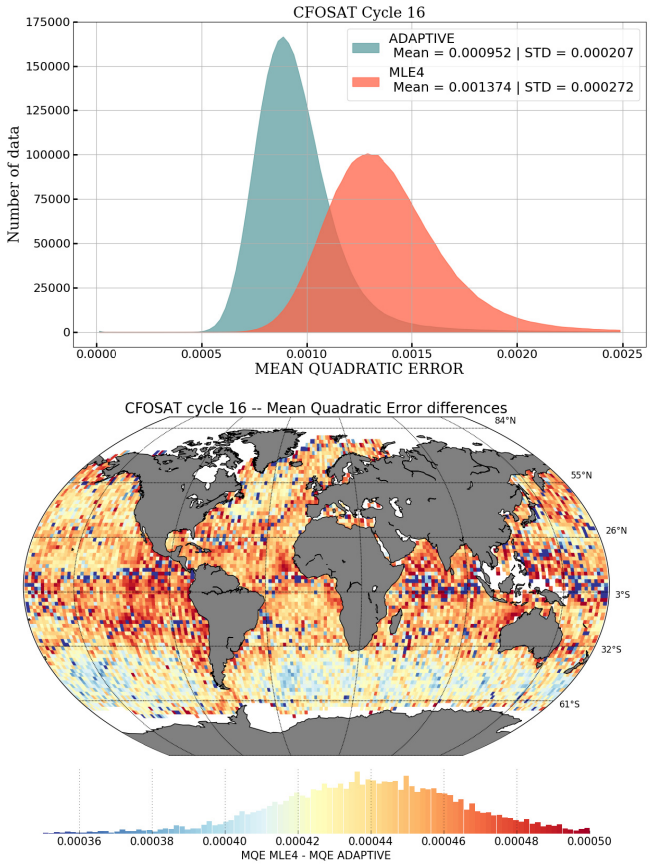

Fig. 6. (Top) Histograms of MQE Adaptive (Blue) and MLE4 (Red) and (Bottom) gridded map of the difference of MQE between MLE4 and Adaptive for CFOSAT cycle 16.

particular at low-to-moderate sea-state conditions. Second, as mentioned before, one interest of the Adaptive method is to better fit nonstandard peaky echoes as observed on highly specular surfaces such as bloom events or marginal ice over the ocean, due to the inclusion of a parameter related to the surface characteristics (namely the square slope mss) in the exponential term in (10).

C. Significant Wave Height

Fig. 7 shows the differences between the SWH parameter (MLE4 or Adaptive) retrieved from altimetry and the ECMWF model, interpolated at the altimeter resolution, over data from cycle #16 (13 days). Both solutions show a low mean bias (∼1 cm for MLE4 and ∼3 cm for Adaptive), confirming that no LUTs are needed for the Adaptive. In addition, the Adaptive measurements show a 40% lower standard deviation compared to the MLE4 solution, which is consistent with the results presented in Section IV.

A spectral analysis on the SWH parameter, performed for MLE4 and Adaptive, is shown in Fig. 8. The spectra are obtained from continuous series of SWH values along track (segments of 700 km long). Noise levels can be computed using the following formula:

$$\text{Noise Level (cm)} = \sqrt{\frac{P_S}{2 * \Delta\tau}}$$

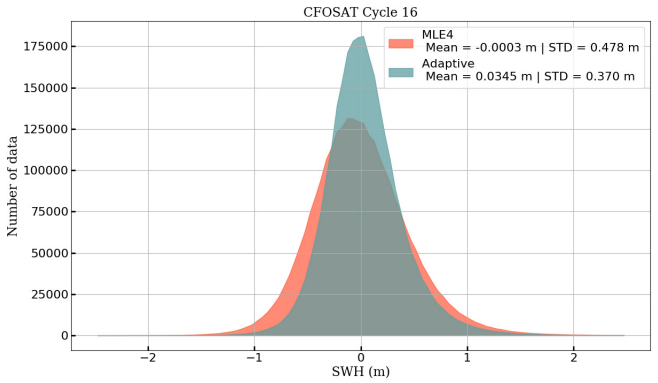

Fig. 7. Histograms of SWH differences between MLE4 (LUTs applied) and ECMWF (orange) and Adaptive (No LUTs) and ECMWF (green) for CFOSAT cycle 16.

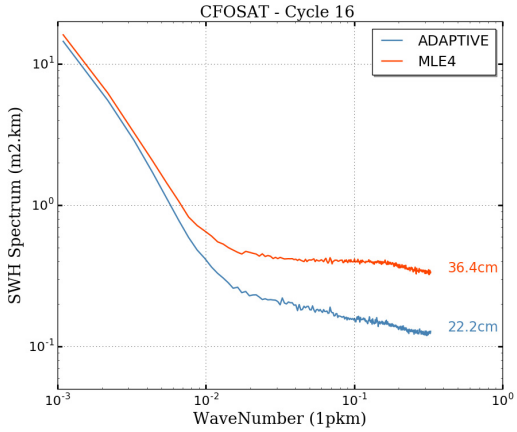

Fig. 8. MLE4 and Adaptive SWH spectral analysis (MLE4 in orange and Adaptive in blue). For the MLE4 spectrum, LUTs are accounted for. Noise levels are computed for both solutions.

where $\Delta\tau$ is the resolution sampling (1.4 km for 5-Hz CFOSAT data) and P_S is the power spectrum computed after the averaging of several individual power spectra obtained on independent data segments [23].

For MLE4, the 5-Hz noise level is equal to 36.8 cm, whereas the Adaptive 5-Hz noise level equal to 21.7cm. Hence, the Adaptive reduces the SWH noise level by 41% compared to the MLE4 solution. The results obtained on simulations (see Section IV) predicted a 60% noise reduction; however, these simulations did not consider the 4.5-Hz sampling rate of the SWIM products, which is not enough to reach the "instrumental plateau" or white noise that can be observed on 20-Hz spectral analysis [24]. A similar comparison, done with Jason-3 data (not shown here), shows a 60% SWH noise reduction. Nevertheless, the current Jason-3 instrumental noise on the SWH parameter, retrieved with MLE4, is around 50 cm [24], meaning that SWIM SWH is 60% less noisy than the current Jason-3 SWH product.

D. Backscattering Coefficient σ^0

Similar to the along-track spectra shown for SWH in Fig. 8, Fig. 9 shows the spectra estimated for the σ^0 parameter. The MLE4 (orange curve) shows a "hump" at specific scales. This is a well-known artifact [24] due to a strong correlation

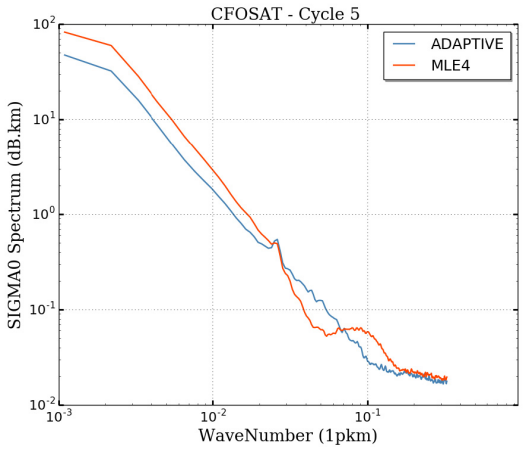

Fig. 9. MLE4 and Adaptive σ^0 spectral analysis (MLE4 in orange and Adaptive in blue).

between the slope of the trailing edge and the σ^0 parameter, in conditions when the MLE4 algorithm is not well suited for retracking echoes departing from the Brown model, such as echoes in rain events, bloom events, and marginal sea ice [4], [23]. In opposite, with the Adaptive algorithm, the σ^0 spectrum is much more continuous. This is because, with the Adaptive model, the σ^0 parameter is constrained by the trailing edge and not only by the amplitude of the echo.

This improvement can be particularly well observed on special events such as a rain event, as shown in Fig. 10. In this example, we can see SWIM nadir echoes impacted by a rain event, characterized by a significant loss in the amplitude of waveforms associated with a decrease in the automatic gain control (AGC) values compared to its classical oceanic value (19 dB for SWIM) [25]. Even though both σ^0 parameters are impacted by the rain event, the Adaptive estimates follow the AGC variations, whereas the MLE4 does not. In the Adaptive algorithm, the echo trailing edge is constrained by the mss (and hence σ^0), which enables σ^0 to follow naturally the amplitude variations of the signal, making it a much better tool compared to the MLE4 to detect specific events such rain as cells. Indeed, as explained in Section III-B, the latter uses a model where the trailing edge of the echo is only constrained by the attitude of the altimeter. In specific events where the surface roughness dominates the trailing edge, the Brown model is thus not a suitable option. Note that a rain flag is defined in the nadir products, using [25]. The preliminary analysis already shows good consistency between this flag and collocated radiometers.

As explained in [9], the introduction of a parameter related to the surface roughness allows the retracking of peaky echoes, characteristic of specular surfaces such as sea ice. This is particularly of interest in the Arctic basin where the diversity of surface types can result in complex waveform shapes and characteristics. Indeed, leads (calm water) and polynyas (new sea ice) are characterized by a highly strong power return. On the other hand, a uniform cover of sea ice will mainly have a stronger signal than ocean, due to the high reflectivity of the sea ice. However, in some areas, the specificities of the ice will imply a received power similar to over ocean, typically at the west of the Arctic basin. The σ^0 values retrieved in the Arctic region are shown in Fig. 11 for the MLE4 and Adaptive algorithms. Fig. 12 shows for the same period the sea-ice concentration parameter extracted from ECMWF [see Fig. 12(b)] and the sea-ice type extracted from the OSISAF website for a specific day during the period [see Fig. 12(a)]. As expected, the σ^0 estimated from MLE4 does not show a good consistency with the sea-ice characteristics: the retrieved σ^0 are lower over sea ice than over the ocean and there is no variation visible in the Arctic basin. This is the consequence of the use of the Brown model, which was defined for fitting ocean-like waveforms only.

In opposite, the σ^0 obtained from the Adaptive retracker [see Fig. 11 (left)] shows a qualitative high consistency with the sea-ice extent [see Fig. 12(b)] and exhibits variations within the Arctic basin consistent with the ice type map of Fig. 12(a), with first-year ice observed in Fig. 12(a) corresponding to the highest values of σ^0. These preliminary results show that the Adaptive model fits well non-Brownian echoes. This opens perspectives for studies on sea-ice surfaces, as well as on scenes affected by rain and/or bloom. Indeed, due to its inclination, CFOSAT reaches a maximum latitude of 82.5° north, making it a good candidate to study the polar areas. As CFOSAT does not give information about topography, it cannot be used to compute the sea-ice freeboard. However, as shown here above, σ^0 values have the potential to characterize sea-ice type, which could lead to multiple sea-ice applications. For instance, it could be used to enrich existing altimeter sea-ice extent data to improve the quality of multimission sea-ice extent products. Also, this work could be linked to analysis on SWIM off-nadir data, which also shows sensitivity to sea-ice type. One operational application would be to replace the current sea-ice detection based on the ECMWF data by an SWIM nadir or combined nadir and off-nadir sigma0 processing.

VI. Quality Assessment of the Adaptive Algorithm Used for SWIM Based on Independent Data Sets

To complete the assessment of the operational SWIM data products that are based on the Adaptive algorithm, we analyze in this section the SWIM nadir data with respect to independent external data sets such as models and conventional altimetric missions.

A. Description of the Data Set

This assessment is based on SWIM L2 nadir products, in operational processing version V4.3.2, more specifically the following parameters given at 5 Hz: *swh_native* and *sigma0_native* derived from the Adaptive algorithm and *wind_native* derived from σ^0 due to the inversion algorithm described in [26]. Results include comparisons to models, interpolated at SWIM resolution as well as comparisons to altimetric missions (Jason-3 and AltiKa). For the latter, a colocation at crossover points was performed by retaining points when distances are less than 7 km along track and time differences are less than 3 h. The cycles chosen for this analysis are cycles 21–28, covering the period from July 28, 2019 to October 1, 2019.

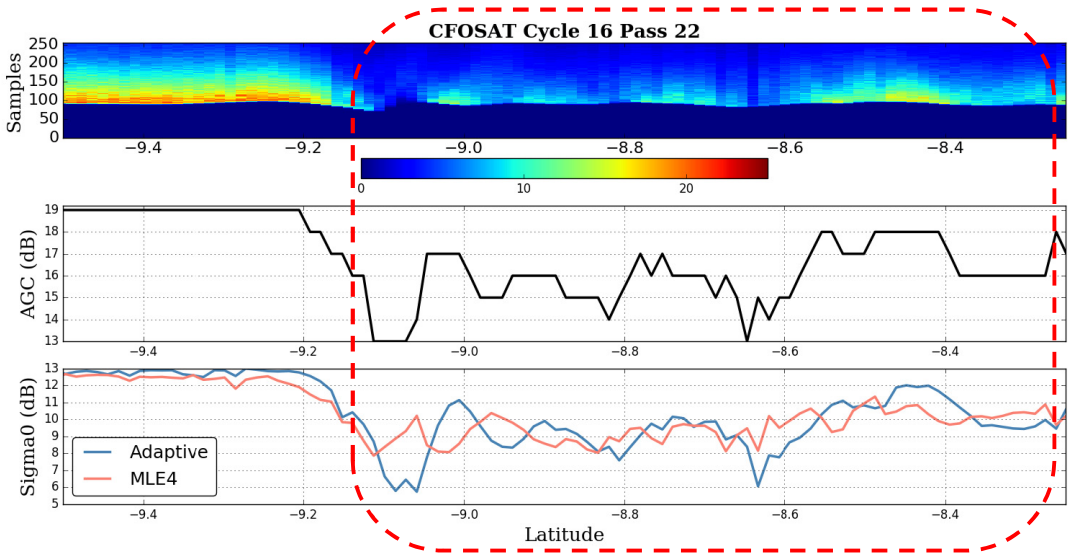

Fig. 10. (From Top to Bottom) Radargram illustrating power in each waveform bin for the chosen section along-track (color indicates intensity), AGC for the same along-track section, and σ^0 for the same along-track section (Adaptive in blue and MLE4 in red). The red dotted box indicates the beginning and end of the rain event.

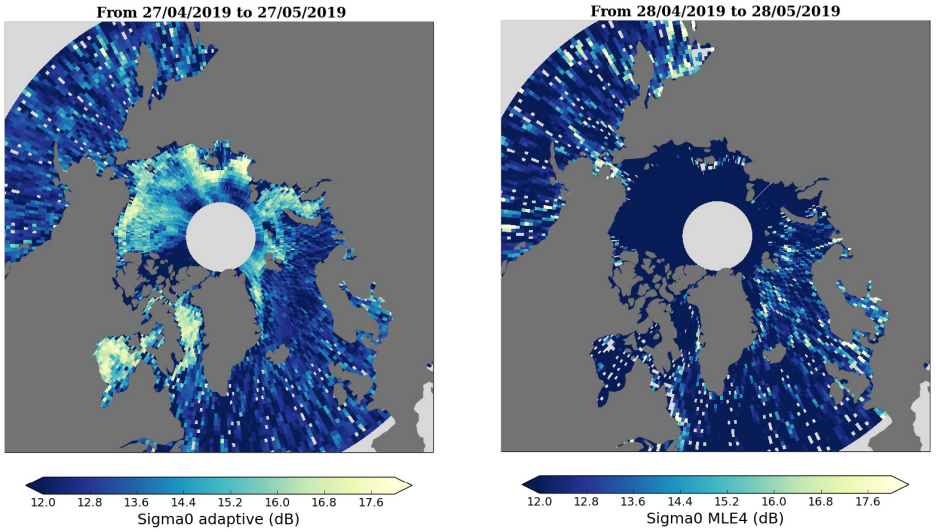

Fig. 11. Gridded maps of (Left) σ^0 Adaptive and (Right) σ^0 MLE4 over 30 days of data.

B. Significant Wave Height

Fig. 13 shows a $2° \times 2°$ gridded comparison of SWIM nadir SWH to ECMWF Hs model. As seen on the histogram on top of the plot, a good agreement is noticed, with a global bias of $\sim$3 cm. The map highlights that the highest bias values can be observed in specific regions corresponding to low and high waves (high latitudes and Indian ocean mostly). Nevertheless, as already shown in [13, Fig. 6], the mean biases are less than 1 cm regardless of the sea state and show a minor positive trend with wave height (from 0 to about 0.5 m for SWH varying from 2 to 7 m) and wind speed (from 0 to 0.2 m for wind speed varying between 2 and 17 m/s). This wave height bias is negative for small SWHs (less than 1 m), null around 2 m height and positive for higher waves (see [13, Fig. 6]).

The comparison to altimetric data from Jason-3 and SARAL/AltiKa also shows a good agreement. Small biases with weak SWH dependencies can be observed in Fig. 14, except for the points below 1 m and above 6 m where the number of crossover points is much smaller. This smaller number of points also induces an increase of the standard deviation around the mean. For this comparison, it is important to note that the SARAL and Jason-3 data sets are based on the MLE4 retracker, corrected using LUTs, whereas SWIM estimates do not need any LUTs, as proved in Sections IV and V.

C. Backscattering Coefficient σ^0 and Wind Speed

As already described in [13], the analysis over data from cycle #23 (from August 14, 2019 to August 26, 2019) has shown the remarkable consistency of the σ^0 parameter

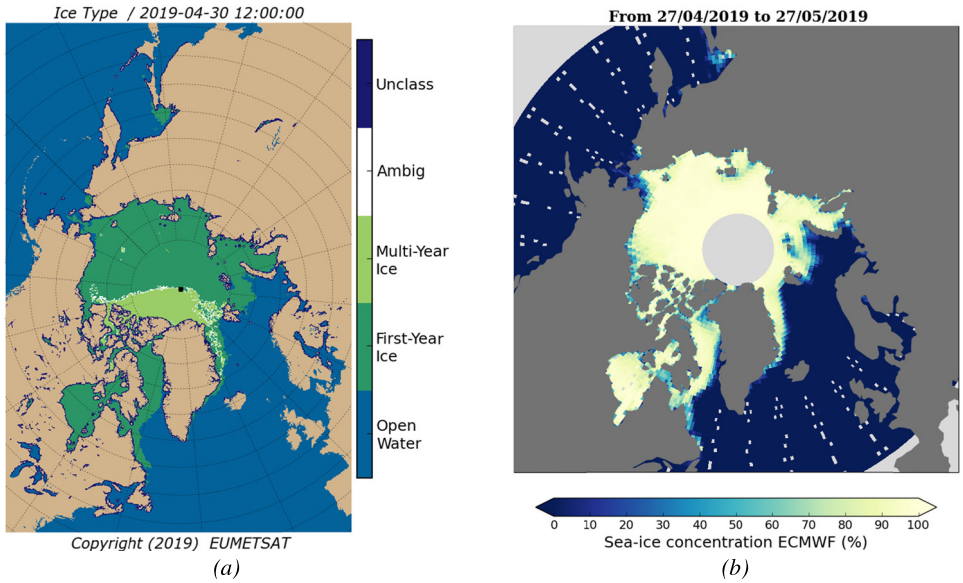

Fig. 12. (a) Daily sea-ice-type map extracted from the OSI-SAF quick-look website (http://osisaf.met.no/p/) for April 30, 2019. (b) Gridded map of sea-ice concentration from ECMWF over 30 days on data.

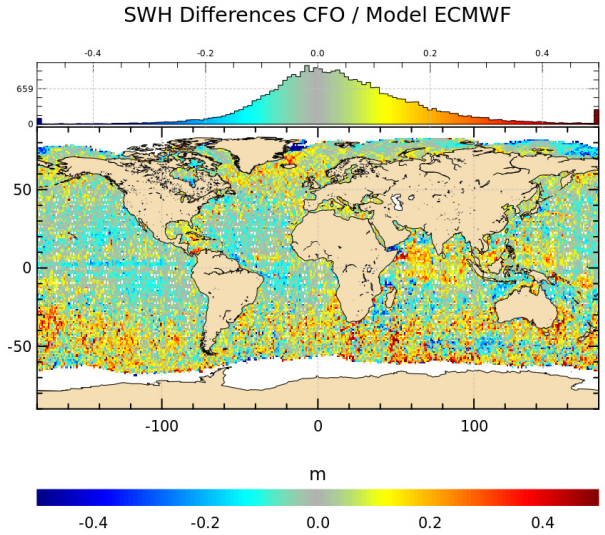

Fig. 13. Difference between SWIM nadir SWH and ECMWF Hs for SWIM cycles 21–24: (Top) map and histogram. Mean = 0.0362 m. Median = 0.0246 m. Standard deviation = 0.1478 m.

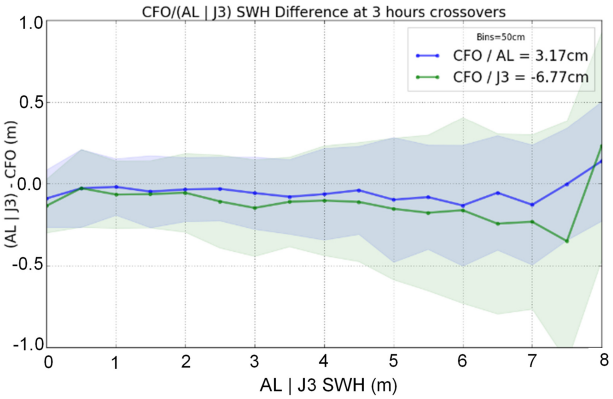

Fig. 14. Bias between SWIM SWH and two altimeter missions (SARAL/AltiKa in blue and Jason-3 in green) for SWIM cycles 21–28. Each dot of the solid line is the mean computed per box of 50 cm of SWH and the envelope represents the associated standard deviation.

between SWIM and Jason-3 altimeter (Poseidon-3B) which is in Ku-band, as SWIM. A mean difference of only 0.12 dB (with 0.4-dB standard deviation) was found in this comparison.

On the other hand, when comparing SWIM results (Ku-band) to AltiKa results (in Ka-band), biases are observed, as described in [13]. They are mainly due to the different responses of the backscattering in Ku with respect to Ka-band.

As opposed to σ^0 (see just above), the winds retrieved from the σ^0 (through empirical relationships relating σ^0 to wind speed and SWH) are directly comparable between altimeters, even for different radar bands, provided that the empirical models used for converting σ^0 into wind speed have been assessed independently. Here, we compare SWIM wind to ECMWF model outputs, AltiKa and Jason-3 data. The wind speed obtained with SWIM is consistent with the ECMWF model wind speed (see Fig. 15). The mean difference is 0.32 m/s, and the standard deviation of the difference is 0.92 m/s. The highest differences are observed in the tropics and at high latitudes. For these areas of extreme Sigma0 values (either very small or high), the differences are likely due to three mixed effects. First, a too smooth ECMWF model does not see all the short-scale variability (mostly in the intertropical zone). Then, a higher uncertainty on wind inversion for poorly represented numerical populations. A new inversion model is planned to be computed again on a longer period to lower this later impact. Finally, although a data selection was applied, some mixed area (sea ice and/or rain) may still locally impact data. This will be further studied and should be reduced in future product version.

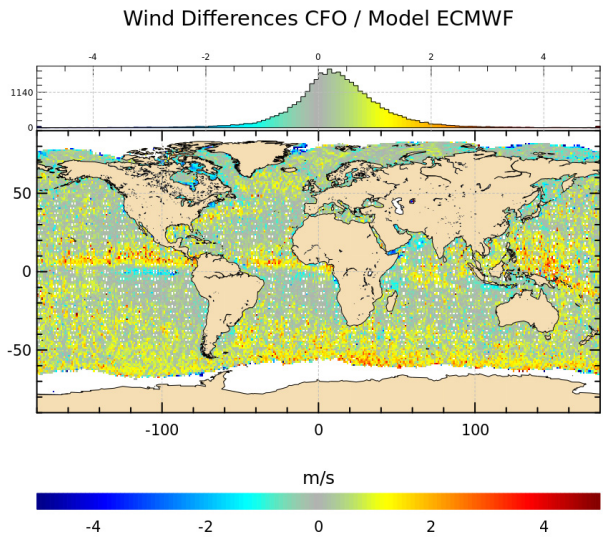

Fig. 15. Difference between SWIM nadir altimeter wind and ECMWF wind for SWIM cycle 21–28: (Top) map and histogram. Mean = 0.32 m/s. Median = 0.30 m/s. Standard deviation = 0.92 m/s.

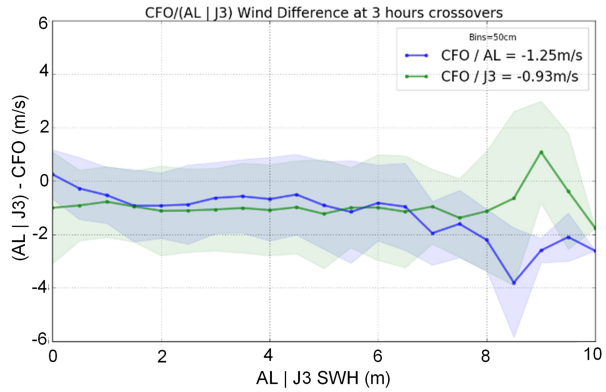

Fig. 16. Bias between SWIM wind and two altimeter missions (SARAL/AltiKa in blue and Jason-3 in green) for SWIM cycles 21–28. Each dot of the solid line is the mean computed per box of 50 cm of SWH and the envelope represents the associated standard deviation.

Compared to the winds provided by Jason-3 and SARAL/AltiKa at crossover points (within 3 h and 7 km, as for Fig. 14), the winds from SWIM are quite consistent, as shown in Fig. 16. The mean differences (around -1 m/s) can be attributed to the σ^0 inversion retrieval algorithms because they differ for each mission. Furthermore, for extreme data (below 1 m and above 6 m), the amount of data is much weaker and the metrics though, less stable. For AltiKa, the algorithm is based on [27], whereas for SWIM, it is estimated from [26]. In the future, a refinement of the model [26] will be proposed based on a 2-D LUT (σ^0 function of wind speed and SWH) as proposed in [28]. It will be carried out using one year of SWIM data to ensure a stable statistical model.

VII. Summary and Conclusion

In this article, we have described and validated the Adaptive algorithm proposed to retrieve the SWH and the normalized radar cross section from radar nadir echoes. We have shown from simulations that compared to the classical MLE4 algorithm, these parameters are retrieved without bias and with less noise (restitution noise reduction of 60% for SWH and 11% for σ^0). As it is not an output of the CFOSAT product, range performances from the Adaptive algorithm have not been detailed in this article. However, significant improvements are also observed for this parameter on oceanic echoes [**?**], and among others, we can note a 10% restitution noise reduction, without any bias.

When applied on real CFOSAT/SWIM data, these improvements ensure the same level of performance over ocean than conventional altimetry missions, despite the SWIM instrument lower measurement rate (4.5 versus 20 Hz). This indicates that for a given noise level on the raw echoes, the geophysical variability can be detected with the Adaptive algorithm at smaller scales than with the MLE4 standard method. This opens the way to higher resolution data analysis from conventional altimetry missions, which will fulfill the need of end users to refine regional models at small scales.

Despite its increased complexity (in particular the numerical convolution with the real PTR), the processing with the Adaptive retracking method is compliant with near real-time production requirements. For example, for CFOSAT, the processing time is approximately 3 min for 105 min of measurements. Other missions could follow this upgrade to improve the whole nadir constellation. As a matter of fact, the Jason future reprocessed products will include products derived from the Adaptive algorithm as an alternative to the MLE4. Both solutions will be available in the products.

In addition, we have shown that the Adaptive algorithm provides improved parameters on specific areas such as sea-ice or rain impacted surfaces, mainly due to the choice of the Amarouche flat surface response model. This latter introduces the mean-square slope of the surface as a parameter of the flat response, allowing to better invert echoes that are different from the Brown model shape. Although no analysis has been done yet on the retrieved mean-square slope parameter, one can presume that it will bring complementary information on the surface roughness characterization, especially for areas where the surface roughness changes rapidly, typically in sea-ice regions, inland waters such as rivers, and specific events such as rain cells and blooms. Due to the improvement of the retrieved parameters, new applications could also be considered over sea-ice surfaces. CFOSAT SWIM nadir products offer a large data set to explore the potential of this processing.

Finally, it should be mentioned that although this study was specifically conducted under the SWIM instrument configuration (simulations) and on SWIM real data, several conclusions are more general and should be considered for improvements in future altimeter data processing or reprocessing, in particular the use of real PTR, allowing the suppression of LUT, and the use of a likelihood estimator instead of an LSE, leading to a reduction of the restitution noise.

Acknowledgment

The authors would like to thank all contributors not mentioned in the list of coauthors: M. Dalila for all her work

on the Surface Waves Investigation and Monitoring (SWIM) databases used for the data analysis presented in this article, F. Andzembe for his implication in the development of the processing chain, N. Tran for her contribution with the wind analysis, L. Amarouche who developed the model used by the Adaptive algorithm, and F. Gouillon for its work and efficiency as the ground-segment development manager.

REFERENCES

[1] G. Brown, "The average impulse response of a rough surface and its applications," *IEEE Trans. Antennas Propag.*, vol. AP-25, no. 1, pp. 67–74, Jan. 1977.

[2] J.-P. Dumont, "Estimation optimale des paramètres altimétriques des signaux radar Poséidon," Ph.D. dissertation, Univ. Toulouse-Enseeiht, Toulouse, France, 1985.

[3] L. Amarouche, P. Thibaut, O. Z. Zanife, J.-P. Dumont, P. Vincent, and N. Steunou, "Improving the Jason-1 ground retracking to better account for attitude effects," *Mar. Geodesy*, vol. 27, nos. 1–2, pp. 171–197, Jan. 2004.

[4] P. Thibaut, J. C. Poisson, E. Bronner, and N. Picot, "Relative performance of the MLE3 and MLE4 retracking algorithms on Jason-2 altimeter waveforms," *Mar. Geodesy*, vol. 33, no. 1, pp. 317–335, Aug. 2010.

[5] D. J. Wingham, C. G. Rapley, and H. Griffiths, "New techniques in satellite altimeter tracking systems," in *Proc. IGARSS Symp.*, Zürich, Switzerland, 1986, pp. 1339–1344.

[6] F. Frappart, S. Calmant, M. Cauhope, F. Seyler, and A. Cazenave, "Preliminary results of ENVISAT RA-2-derived water levels validation over the Amazon basin," *Remote Sens. Environ.*, vol. 100, no. 2, pp. 252–264, Jan. 2006, doi: 10.1016/j.rse.2005.10.027.

[7] B. Legresy, F. Papa, F. Remy, G. Vinay, M. van den Bosch, and O.-Z. Zanife, "ENVISAT radar altimeter measurements over continental surfaces and ice caps using the ICE-2 retracking algorithm," *Remote Sens. Environ.*, vol. 95, no. 2, pp. 150–163, Mar. 2005.

[8] M. Passaro, P. Cipollini, S. Vignudelli, G. D. Quartly, and H. M. Snaith, "ALES: A multi-mission adaptive subwaveform retracker for coastal and open ocean altimetry," *Remote Sens. Environ.*, vol. 145, pp. 173–189, Apr. 2014.

[9] J.-C. Poisson, G. D. Quartly, A. A. Kurekin, P. Thibaut, D. Hoang, and F. Nencioli, "Development of an ENVISAT altimetry processor providing sea level continuity between open ocean and arctic leads," *IEEE Trans. Geosci. Remote Sens.*, vol. 56, no. 9, pp. 5299–5319, Sep. 2018.

[10] D. Hauser, D. Xiaolong, L. Aouf, C. Tison, and P. Castillan, "Overview of the CFOSAT mission," in *Proc. IGARSS*, Beijing, China, Jul. 2016, pp. 5789–5792.

[11] D. Hauser, C. Tison, T. Amiot, L. Delaye, N. Corcoral, and P. Castillan, "SWIM: The first spaceborne wave scatterometer," *IEEE Trans. Geosci. Remote Sens.*, vol. 55, no. 5, pp. 3000–3014, May 2017, doi: 10.1109/TGRS.2017.2658672.

[12] X. Dong, D. Zhu, W. Lin, H. Liu, and J. Jiang, "A Ku-band rotating fan-beam scatterometer: Design and performance simulations," in *Proc. IEEE Int. Geosci. Remote Sens. Symp.*, Jul. 2010, pp. 1081–1084.

[13] D. Hauser *et al.*, "New observations from the SWIM radar on-board CFOSAT: Instrument validation and ocean wave measurement assessment," *IEEE Trans. Geosci. Remote Sens.*, vol. 59, no. 1, pp. 5–26, Jan. 2021, doi: 10.1109/TGRS.2020.2994372.

[14] P. Thibaut, L. Amarouche, O. Z. Zanife, N. Steunou, P. Vincent, and P. Raizonville, "Jason-1 altimeter ground processing look-up correction tables," *Mar. Geodesy*, vol. 27, nos. 3–4, pp. 409–431, Jul. 2004.

[15] G. Hayne, "Radar altimeter mean return waveforms from near-normal-incidence ocean surface scattering," *IEEE Trans. Antennas Propag.*, vol. AP-28, no. 5, pp. 687–692, Sep. 1980.

[16] L. Amarouche, "Contribution à l'étude du biais d'état de mer," Ph.D. dissertation, Universite Paris Denis Diderot, Paris, France, 2001.

[17] L. Amarouche, E. Thouvenot, B. Chapron, and O.-Z. Zanife, "A new estimator of the sea state bias using a three frequency radar altimeter," in *Proc. IEEE Int. Conf. Geosci. Remote Sens. (IGARSS)*, Sydney, NSW, Australia, Jul. 2001, pp. 2510–2512.

[18] J. MacArthur, "SEASAT—A radar altimeter design description," Appl. Phys. Lab., Johns Hopkins Univ., Baltimore, MD, USA, Tech. Rep., 1978.

[19] L. Amarouche, S. Jourdain, and J. R. Deboer, "Rapport Tâche 2.2: Retracking spécifique cellules de pluie et blooms," CNES, Toulouse France, Tech. Rep. SALP-NT-P-EA-21776-CLS, 2010.

[20] L. Amarouche and A. Vernier, "New methods for retracking altimeter sea ice and ice sheets waveforms," ESA, Toulouse France, Tech. Rep. CLS-DOS-NT-10-192, 2011.

[21] A. Halimi, "From conventional to delay/Doppler altimetry," Ph.D. dissertation, Inst. Nat. Polytechnique de Toulouse, Toulouse, France, 2013.

[22] J. A. Nelder and R. Mead, "A simplex method for function minimization," *Comput. J.*, vol. 7, no. 4, pp. 308–313, Jan. 1965.

[23] P. G. Chalenor and M. A Srokoez, "The extraction of geophysical parameters from radar altimeter return from a non-linear sea surface," in *Mathematics in Remote Sensing*, S. R. Brooks, Ed. Oxford, U.K.: Clarendon, 1989.

[24] G. Dibarboure *et al.*, "Investigating short-wavelength correlated errors on low-resolution mode altimetry," *J. Atmos. Ocean. Technol.*, vol. 31, no. 6, pp. 1337–1362, Jun. 2014.

[25] J. Tournadre, J. C. Poisson, N. Steunou, and B. Picard, "Validation of AltiKa matching pursuit rain flag," *Mar. Geodesy*, vol. 38, no. 1, pp. 107–123, Sep. 2015, doi: 10.1080/01490419.2014.1001048.

[26] J. Gourrion *et al.*, "A two-parameter wind speed algorithm for Ku-band altimeters," *J. Atmos. Ocean. Technol.*, vol. 19, no. 12, pp. 2030–2048, 2002, doi: 10.1175/1520-0426(2002)019<2030:ATPWSA>2.0.CO;2.

[27] J. Lillibridge, R. Scharroo, S. Abdalla, and D. Vandemark, "One- and two-dimensional wind speed models for Ka-band altimetry," *J. Atmos. Ocean. Technol.*, vol. 31, no. 3, pp. 630–638, Mar. 2014, doi: 10.1175/JTECH-D-13-00167.1.

[28] F. Collard, "Algorithmes de vent et période moyenne des vagues JASON à base de réseaux de neurons," Boost Technol., Brest, France, Tech. Rep. BO-021-CLS-0407-RF, 2005.

[29] P. Thibault *et al.*, "Adaptive retracker for conventional altimeter echoes: Physical basics and main performances obtained on Jason-3 GDR-F dataset," *IEEE Trans. Geosci. Remote Sens.*, to be published.

Cédric Tourain received the one-year master's degree in space technology from the Université de Méditerranée Aix-Marseille II, Marseille, France, in 2000, and the advanced master's degree in aerospace mechanics and propulsion from the École Nationale Supérieure de l'Aéronautique et de l'Espace, Toulouse, France, in 2001.

He first worked on flight dynamics systems with the Space Department, Thales Services, Toulouse. He moved to DORIS system exploitation in 2005, first as a System Integrity Manager with Collecte Localisation Satellite (CLS), Ramonville Saint-Agne, France, and then as a DORIS Exploitation Expert with the Centre National d'Etudes Spatiales (CNES, the French Space Agency), Toulouse, in 2009. In 2015, he moved to the China France Oceanography Satellite (CFOSAT) Project with the Radar Processing and Products Department, CNES. He coordinates CFOSAT products' processing definition and validation, and since 2019, he has been the CNES CFOSAT Project Scientist.

Fanny Piras received the Engineering degree in geophysics from the Ecole et Observatoire des Sciences de la Terre, Strasbourg, France, in 2014.

Since 2015, she has been with the Spatial Observations Division, Nadir Observations Department, Collecte Localisation Satellites, Toulouse, France. She has been conducting several studies devoted to the analysis and development of methods and algorithms for processing both conventional and synthetic aperture radar nadir altimetry data. She is also involved in the performance monitoring of the different in-flight radar altimeters.

Annabelle Ollivier received the Ph.D. thesis in signal processing dedicated to altimetric noise reduction algorithms in 2006, after engineering studies at the National Polytechnique Institute of Grenoble (INPG), Grenoble, France.

Since then, she has been working on validation and valorization thematics for many altimetric mission projects (lead by ESA, CNES, or JPL) at Collect Localisation Satellite (CLS), Toulouse, France. She is part of the CalVal Group, China France Oceanography Satellite (CFOSAT), mission dedicated to the global measurement of wind and waves from satellite, as a project manager for the Systematic Calval Team to assess these metrics.

Danièle Hauser (Member, IEEE) received the Ph.D. thesis in meteorology in 1980 and a State thesis in physics in 1989.

She is a Senior Scientist with the Centre National de la Recherche Scientifique (CNRS), Guyancourt, France, and develops her research activity at the Laboratoire Atmosphère, Milieux, Observations Spatiales (LATMOS), Guyancourt. She is working on microwave observations of the ocean surface (surface wind, waves, and salinity) and air/sea interaction studies, for more than 25 years. She is also a Principal Investigator of the China France Oceanography Satellite (CFOSAT) Mission dedicated to the global measurement of wind and waves from satellite.

J. C. Poisson, photograph and biography not available at the time of publication.

F. Boy, photograph and biography not available at the time of publication.

P. Thibaut, photograph and biography not available at the time of publication.

L. Hermozo, photograph and biography not available at the time of publication.

C. Tison, photograph and biography not available at the time of publication.